LaserGuider: A Laser Based Physical Backdoor Attack against Deep Neural Networks[*]

Yongjie Xu[**][1][0000−0001−5816−8031], Guangke Chen[**][2][0000−0001−8277−3119], Fu Song[✉][3,4][0000−0002−0581−2679], and Yuqi Chen[1][0000−0003−2988−6012]

[1] ShanghaiTech University {xuyj,chenyq}@shanghaitech.edu.cn
[2] Pengcheng Laboratory chengk@pcl.ac.cn
[3] Key Laboratory of System Software (Chinese Academy of Sciences) and State Key Laboratory of Computer Science, Institute of Software, Chinese Academy of Science
[4] Nanjing Institute of Software Technology songfu@ios.ac.cn

Abstract. Backdoor attacks embed hidden associations between triggers and targets in deep neural networks (DNNs), causing them to predict the target when a trigger is present while maintaining normal behavior otherwise. Physical backdoor attacks, which use physical objects as triggers, are feasible but lack remote control, temporal stealthiness, flexibility, and mobility. To overcome these limitations, in this work, we propose a new type of backdoor triggers utilizing lasers that feature long-distance transmission and instant-imaging properties. Based on the laser-based backdoor triggers, we present a physical backdoor attack, called LaserGuider, which possesses remote control ability and achieves high temporal stealthiness, flexibility, and mobility. We also introduce a systematic approach to optimize laser parameters for improving attack effectiveness. Our evaluation on traffic sign recognition DNNs, critical in autonomous vehicles, demonstrates that LaserGuider with three different laser-based triggers achieves over 90% attack success rate with negligible impact on normal inputs. Additionally, we release LaserMark, the first dataset of real-world traffic signs stamped with physical laser spots, to support further research in backdoor attacks and defenses.

Keywords: Backdoor attacks, data poisoning, DNNs, laser, physical attacks

1 Introduction

Recently, deep neural networks (DNNs) have been widely deployed in various applications such as autonomous driving [21], medical diagnosis [2], media understanding [20, 32], and attack detection [3]. While their success is attributed to increasingly complex structures and large capacities, DNNs require substantial data and computation for training. This has led to a growing reliance on

---

[*] In Proceedings of the 23rd International Conference on Applied Cryptography and Network Security (ACNS), Munich, Germany, 23-26 June, 2025

[**] Co-first authors & equal contribution, where the order is determined by a random coin flip.

third-party datasets, platforms, or pre-trained DNNs [25], introducing vulnerabilities to backdoor attacks [7,8,16,27,31,44,49,52–54]. Backdoor attacks aim to embed hidden associations between triggers and targets into DNNs during training. During inference, DNNs misclassify inputs with triggers to attacker-specified targets while performing normally on inputs without triggers.

In reality, DNNs are invocated as follows: physical objects are captured as analog signals by sensors, converted to digital inputs, and then fed into DNNs for prediction. Early digital backdoor attacks assume direct manipulation of digital inputs [7,10,16,28–30,33,35,44,50,55], making them less effective or infeasible in real-world scenarios. Later attacks adopt physical triggers to manipulate physical objects to activate backdoors [7,16,26,47], improving practicality. However, current physical backdoor attacks face limitations: lack of remote control ability, low temporal stealthiness, and low flexibility and mobility (see Section 3.3).

We observe that these limitations are attributed to that their adopted physical triggers (e.g., square stickers [16], sunglasses [7], and earrings [47]) have to be physically attached onto the physical objects. This motivates us to design a new type of physical triggers. After investigation, we choose laser spots as physical triggers, due to its notable advantages as follows: (1) Laser possesses the long-distance transmission ability, thus can be projected to the physical objects remotely. (2) Laser possesses the instant-imaging capability, thus the adversary can turn on a laser pointer to project the laser onto a physical object *right before* the physical object got captured by sensors, achieving high temporal stealthiness. (3) The projection position can be instantaneously switched from one physical object to another object, achieving high flexibility and mobility during a consecutive attack.

Based on our novel laser-based triggers, we propose a physical backdoor attack, named LASERGUIDER. LASERGUIDER embeds backdoors by poisoning training datasets. To reduce the cost of collecting training samples with physical laser spots, we simulate physical triggers using digital laser-based triggers, which are used to poison clean digital samples. We also propose an effective approach to optimize these digital triggers with adjustable parameters to achieve more powerful physical backdoor attacks.

We evaluate LASERGUIDER on state-of-the-art traffic sign recognition DNNs commonly used in autonomous driving [14,16]. Experiments on a self-collected real-world dataset with physical laser spots confirm that LASERGUIDER achieves 90.5%, 93.2%, and 95.3% attack success rates with three types of laser-based triggers (differing in color and shape) while negligibly impacting normal inputs. Additionally, LASERGUIDER supports many-to-one and many-to-many backdoor attacks, allowing multiple triggers to activate the same or distinct backdoors. An ablation study further validates the effectiveness and generalizability of our laser parameter optimization approach.

In summary, the main contributions of this work are:

– We design a new type of laser-based backdoor triggers based on which we propose a physical backdoor attack LASERGUIDER, featuring remote control

ability, high temporal stealthiness, and high flexibility and mobility, thanks to the unique properties of lasers.
- We propose a systematic approach to optimize the parameters of laser-based triggers, enhancing the attack success rate of our physical backdoor attack.
- We capture, collect, and clean traffic sign images with physical laser-based triggers in the real-world, and release them as the first public dataset Laser-Mark to facilitate further research in this field.

Organization. Section 2 covers background and related work on backdoor attacks. Section 3 introduces our backdoor attack LASERGUIDER, including the threat model (Section 3.1), overview (Section 3.2), laser-based trigger design (Section 3.3), and laser parameters optimization approach (Section 3.4). Section 4 details the experimental setup, especially our publicly available dataset, LaserMark. Evaluation results are presented in Section 5. Section 6 discusses failure cases and potential countermeasures. Section 7 finally concludes the work.

Acronyms. We summarize in Table 1 the acronyms used in this work. Our code and dataset are available at `https://github.com/S3L-official/LaserGuider`.

Table 1: Main acronyms.

Acronym	Description
T_{train}	clean training dataset
T_{test}	clean test dataset
P_{train}	poisoned training dataset with digital triggers
P_{test}	poisoned test dataset with physical triggers
$T_{select}; \alpha$	selected subset of T_{train} for adding digital triggers; $\alpha = \frac{|T_{select}|}{|T_{train}|}$
$x; \delta; x^{\delta}; y; y^t$	image; trigger; image with trigger; label; target label
A_p/A_{pn}	portion of images in P_{test} which are classified as the target label on poisoned/normal models
A_c/A_{cn}	portion of correctly classified images in T_{test} on poisoned/normal models

Ethical Considerations. (1) *Strictly Controlled Experiments:* We targeted open-source models and ensured our attack evaluation caused no real-world harm. Poisoned datasets and models were not released online. (2) *Discussion of Countermeasures:* We discuss countermeasures in Section 6.2 to mitigate potential threats, offering insights for stronger defenses.

2 Background & Related Works

2.1 Backdoor Attacks

Backdoor attacks on DNNs insert secret associations between triggers and targets into DNNs so that they perform normally on inputs without triggers, but

behave maliciously as the adversary intended in the presence of a designated trigger. The feasibility of such attacks lies in the loss of control over training and/or training datasets, e.g., adopting third-party datasets instead of collecting and annotating own training dataset, using third-party training platforms instead of training locally, and even directly deploying third-party pre-trained DNNs rather than training from scratch [25].

Backdoor can be embedded in various different ways, such as poisoning training datasets [16, 47], modifying the model parameters [36], or adding extra submodules [42], among which training dataset poisoning is the most typical and widely adopted strategy [25]. Specifically, the adversary creates a poisoned training dataset by mixing normal samples with poisoned samples, where each poisoned sample consists of a data point with a designated trigger and a target label chosen by the adversary. Training on such poisoned dataset results in a backdoored DNN with the adversary-chosen behavior in the presence of triggers. During inference, the adversary attaches a trigger to the input sample to activate the backdoor, forcing the DNN to behave maliciously as intended.

2.2   Related Works

Current backdoor attacks can be broadly categorized into digital backdoor attacks and physical backdoor attacks.

Digital backdoor attacks. Such attacks [7, 10, 16, 28–30, 33, 35, 39, 40, 44, 50, 55] assume that the adversary can manipulate DNNs' digital inputs to insert triggers. While well-explored, this assumption limits their real-world applicability, where physical inputs are captured by sensors and converted to digital form, preventing direct manipulation. This motivates our focus on physical backdoor attacks.

Physical backdoor attacks. In physical attacks, the adversary manipulates physical inputs to influence digital ones, using objects as backdoor triggers, such as square stickers [16], sunglasses [7], and earrings [47]. These triggers activate the backdoor during inference by attaching them to physical objects, like placing a sticker on a traffic sign for traffic sign recognition DNNs [16] or wearing sunglasses for face recognition DNNs [47]. While more practical than digital attacks, current physical backdoor methods suffer from limitations in remote control, temporal stealthiness, flexibility, and mobility. We propose a laser-based physical backdoor attack to address these limitations.

Attacks based on lighting & laser. In [23], an LED-based color stripe pattern is utilized as a backdoor trigger. The LED parameters (e.g., intensity) are optimized using evolutionary computing based on the target DNN's predictions. Their attack targets the unique registration phase of face recognition by embedding patterns into the victim's registered face and the adversary's face captured by cameras, causing the DNN to misidentify the adversary as the victim. In contrast, our attack impacts the training phase by poisoning training datasets, offering a broader model and application scenario generalizability. In addition, their attack still lacks remote control ability and suffers from low feasibility since

the LED needs to be placed very close to the physical objects and the cameras, and has to be placed ahead over each physical object to be attacked.

Another related work, AdvLB [14], projects laser beams onto physical objects to create adversarial examples that fool DNNs including autonomous driving. AdvLB optimizes laser parameters using greedy methods. The key differences are: (1) AdvLB focuses on inference-phase adversarial attacks, while LASER-GUIDER targets training-phase backdoor attacks; and (2) AdvLB uses laser beams, whereas LASERGUIDER employs laser spots, involving distinct laser parameters.

3   Methodology of LASERGUIDER

3.1   Threat Model

Adversary's goal. Backdoor attacks aim to make victim DNNs behave as intended by adversaries when triggers are present, with varying goals depending on DNNs' application scenarios, such as traffic sign recognition [14, 16], face recognition [23, 47], person re-identification [38], lane detection [17, 51], OCR [9], and pedestrian detection [38]. For example, in traffic sign recognition, a stop sign with a trigger may be misclassified as a speed limit sign, causing potential car collisions. In face recognition, the face of imposters (resp. victims) with triggers may be recognized as from victims (resp. imposters), causing authentication bypass (resp. DoS). LASERGUIDER, is general and applicable across scenarios. Following prior works [4, 11, 12, 14, 16, 19, 24, 34, 37, 48], we evaluate it using traffic sign recognition as a case study, a critical and widely used component in autonomous driving. While adversaries may lack direct financial motivation to target self-driving cars [5], traffic sign recognition adequately evaluates the attack.

Meanwhile, the adversary intends to achieve stealthiness and mobility. The stealthiness is two-fold: (1) the victim DNNs should maintain sufficient performance on normal inputs without triggers, otherwise they will be discarded; (2) the trigger adding and removal should leave attack evidence as little as possible. Existing physical backdoor attacks typically necessitate close proximity to the targeted physical objects and sufficient time slots before and after the attack to add and remove the triggers, respectively, significantly heightening the exposure risk. Mobility means triggers can be added conveniently and efficiently to multiple physical objects for consecutive and real-time attacks, unlike existing methods requiring the pre-deployment of triggers to multiple traffic signs.

Adversary's capability. Firstly, we assume that the adversary can manipulate a dataset and upload the resulting dataset online, which will be downloaded and used for training DNNs by developers. However, the adversary cannot *modify* any other aspects of training such as DNN architecture and training algorithm. Accordingly, the adversary chooses to insert the backdoor by poisoning training datasets instead of modifying DNN parameters or adding malicious sub-modules. Despite this, the adversary may *know* the details of target DNNs. This is reasonable considering the wide adoption of public well-known model architectures

and typical training algorithms (e.g., Adam [22]). Secondly, the adversary cannot directly modify the digital inputs when launching attacks at inference time, so needs to launch physical backdoor attacks by manipulating the physical objects. Regarding the physical attack, we assume that the adversary cannot touch the physical objects to add or remove any triggers, e.g., many traffic signs are erected in high places, the adversary cannot touch the face of victims for causing DoS. Despite this, the adversary can maintain a reasonable distance from the physical objects such that the physical objects can be recognized by the adversary and projected by common lasers.

3.2   Overview of LASERGUIDER

The overview of our attack LASERGUIDER is depicted in Fig. 1, consisting of two stages, namely, backdoor embedding and backdoor triggering.

Backdoor embedding. This stage injects a backdoor into DNNs by poisoning the training dataset, following the common practice of previous backdoor attacks [7,10,16,28–30,33,44,55]. First, the adversary specifies a target label y^t and designs a *digital* laser-based trigger δ (cf. Section 3.3). Then, he selects a subset T_{select} of images from a legitimate training dataset $T_{train} = \{(x_i, y_i)\}_{i=1}^N$ where $\alpha = \frac{|T_{select}|}{|T_{train}|}$ is a small ratio, and adds the trigger δ to each image x in the chosen subset T_{select} and associates each modified image x^δ with the target label y^t, obtaining the poisoned training dataset $P_{train} = T_{train} \cup \{(x^\delta, y^t)|x \in T_{select}\}$ Finally, the adversary publishes the poisoned dataset on the Internet, waiting for developers to download the dataset for training their DNNs, during which the backdoor will be naturally embedded into DNN models as a result of training with the poisoned dataset. The dataset poisoning scheme enables our attack to process inherent model generalizability, i.e., the poisoned training dataset can be used by and affect any model. We will test our attack on four different models in Section 5. Compared with previous backdoor attacks, LASERGUIDER features the laser-based trigger, the design of which will be elaborated in Section 3.3.

Backdoor triggering. This stage activates the embedded backdoor in victim DNN models by adding *physical* laser-based triggers to physical objects. To achieve this goal, the adversary simply turns on a laser pointer and projects the laser onto the targeted physical object, e.g., traffic sign in this work, to which the autonomous vehicle equipped with the backdoored DNN model is going to photograph, forcing it to make a wrong prediction. To terminate the attack and destroy the attack evidences for being noticed, the adversary only needs to turn off the laser pointer. Moreover, during attack, the adversary is free to change the irradiation angle and orientation of the laser pointer, so that the laser spot can be quickly transferred and switched on the nearby traffic signs to achieve real-time and consecutive attacks, which significantly improve the attack efficiency considering the high mobility of autonomous vehicles. All these operations can be performed remotely with a reasonable distance from traffic signs and autonomous vehicles.
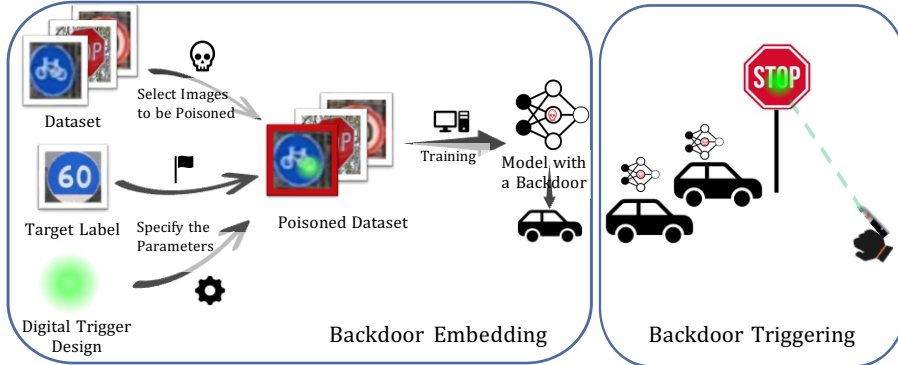
Fig. 1: Overview of LASERGUIDER.

3.3 Trigger Design

Design motivation. Existing physical backdoor attacks utilize various physical objects as triggers, e.g., square [16], earrings [47], sunglasses [7], bandana [47], and tattoo [47]. These triggers are typically deployed in a "sticker-pasting" setting [14], where the adversary prints the triggers as stickers and affixes them onto physical objects. Because of the "sticker-pasting" setting, these backdoor attacks suffer from the following three limitations:

- **Lack of remote control ability**. To control (e.g., adding or removing) triggers, physical objects are required to be physically accessible to the adversary so that the adversary can move close enough to touch and manipulate them. This is inconvenient and is not always possible in practice, e.g., many road traffic signs are erected on high places. e.g., adversaries cannot touch victims' face for causing DoS. Also, the physical presence of the adversary increases the risk of being noticed by victims and defenders.
- **Low temporal stealthiness**. The trigger must be pasted to the targeted physical object in advance. This typically leaves a sufficient time gap before the sensor captures the targeted physical objects [14], definitely increasing the risks of attacks being detected and subsequently removed.
- **Low flexibility and mobility**. The adversary attempts to achieve a consecutive attack where the victim DNN will be affected by multiple physical objects or the same physical object with different triggers. Existing attacks require multiple triggers to be added *in advance* into the physical objects that are likely to be captured, reducing flexibility, mobility, and efficiency.

We remark that these limitations are general across DNNs' application scenarios (at least for those in Section 3.1). For face recognition, they pose no issue for causing authentication bypass but are crucial for causing DoS. Even LED-based triggers [23], which avoid "sticker-pasting", still suffers from these limitations (cf. Section 2.2).

This work is motivated by the following question: "*how to design a backdoor trigger to enable a backdoor attack with better stealthiness, convenience, efficiency, flexibility, and mobility in the physical real-world?*"

Design. After investigation, in this work, we propose to use laser spots as physical triggers due to their unique and desirable properties as follows.

Firstly, lasers have high brightness and exhibit highly collimated propagation without significant divergence, hence can maintain high power density even after a long-distance transmission. As a result, the adversary can manipulate the targeted physical objects by projecting lasers onto them from a long distance, *achieving remote control ability.*

Secondly, as the swiftest entity in the world, lasers possess the instant-imaging property, i.e., there is a very short delay between the moment the laser is emitted from the laser pointer and when it is projected onto the intended targeted physical object. Hence, the adversary can launch the attack in a blink right before the targeted physical object is captured by the imaging sensor by simply turning on a laser pointer emitting the laser, rather than deploying the attack in advance, *achieving high temporal stealthiness.* Also, to launch consecutive attacks, the adversary can simply move the projection of lasers from one physical object to nearby ones by simply switching the laser pointer's projection position or using multiple laser pointers, *achieving high flexibility and mobility.*

Lastly, lasers exhibit exceptional anti-interference capabilities and formidable penetrating power. As a result, the triggers and attacks possess a remarkable resilience against environmental disturbances, such as intense light, rainfall, and fog. This ensures their unwavering effectiveness even in challenging conditions.

Digital & physical laser-based triggers. To obtain the poisoned training data, the adversary can photograph physical objects projected with physical laser-based triggers in the real world. However, this involves substantial labor effort. Therefore, when constructing a poisoned training dataset, we use digital laser-based triggers to simulate the patterns of physical triggers. Specifically, given the specified laser spot color and shape, it is easy to create a digital trigger that fulfills the requirements through geometric drawing.

In this work, we demonstrate our attack using three types of laser pointers, whose laser spots are shown in the first row of Fig. 2, with three different colors (i.e., red, green, and blue) and two different shapes (e.g., circle and rectangle). The second and third rows show the traffic signs with digital and physical triggers, respectively. The digital triggers are very close to the physical triggers. In Section 5, we will empirically show that DNNs trained with digital trigger poisoned dataset are highly susceptible to the attack with physical triggers, and poisoning training datasets using digital triggers does not reduce the attack success rate compared to utilizing physical triggers.

3.4   Optimization of Physical Backdoor Attack

Although digital laser-based triggers can be created to share the same laser spot color and shape with the physical triggers specified by the adversary, there

(a) Triggers

(b) Traffic signs with digital triggers
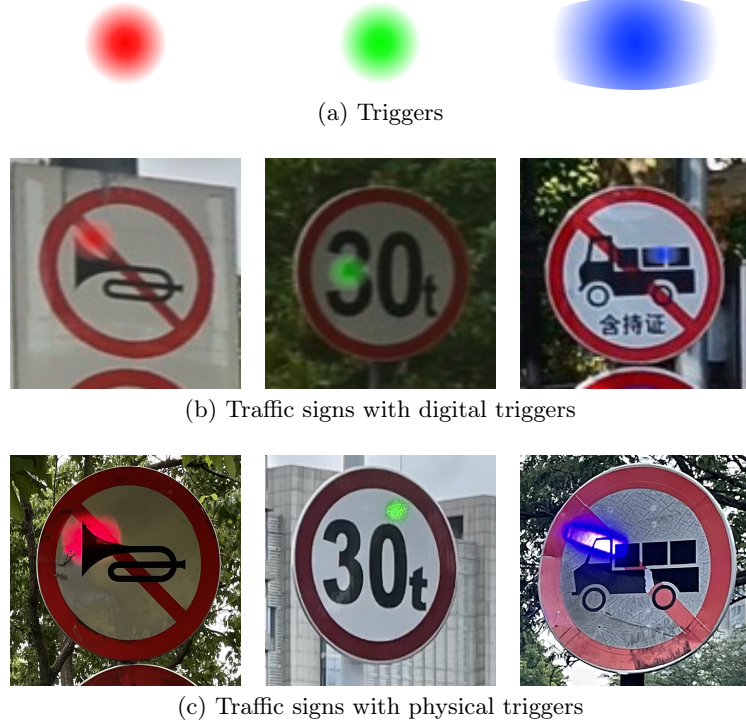

(c) Traffic signs with physical triggers

Fig. 2: Digital and physical laser-based triggers

remains other laser parameters that need to be considered, such as the laser spot size, transparency, location w.r.t. traffic signs, and whether the laser spot center is highlighted. These laser parameters may influence the performance of LASERGUIDER, so we need to carefully specify their values for the digital triggers prior to constructing the poisoned digital training datasets.

To solve the above problem, we propose an effective approach to automatically and efficiently optimize these laser parameters towards a more powerful attack. As shown in Algorithm 1, it mainly consists of two phases, namely, deciding the order of optimizing laser parameters (Lines 1-8) and optimizing the laser parameters according to the optimization order (Lines 9-14).

The effects of these laser parameters on the physical attack may vary and be coupled, namely, the adjustment of one laser parameter may affect the optimal value of other laser parameters. To address this challenge, we first determine the optimization order of them in the first phase according to their degree of impact (i.e., impact factor) on the attack success rate. Specifically, we first randomly select a valid value from its value range R_i for each laser parameter, based on which a baseline victim model M_0 is trained and its attack success rate A_p^0 is evaluated. Then for each laser parameter, we randomly select another random value different from the initialized value while the values of other laser param-

---

Algorithm 1 Optimizing laser parameters

Input: Laser parameters to be optimized $\mathcal{V} = \{\cdots, V_n\}$; Value range of each laser
    parameter $\mathcal{R} = \{\cdots, R_n\}$; Local model $\mathcal{M}$; Clean training dataset T_{train}; Poisoned
    test dataset P_{test}
Output: Optimized values of laser parameters
 1: **for** i from 1 to n **do**
 2:    $S_0[V_i] \leftarrow$ select a random value in the value range R_i
 3: $A_p^0 \leftarrow$ `Evaluate`(S_0); $E \leftarrow \emptyset$
 4: **for** i from 1 to n **do**
 5:    $S \leftarrow S_0$
 6:    $S[V_i] \leftarrow$ select another random value in the value range $R_i \setminus \{S[V_i]\}$
 7:    $A_p^i \leftarrow$ `Evaluate`(S); $E \leftarrow E \cup \{|A_p^0 - A_p^i|\}$
 8: Defining $j_i, i = 1, \cdots, n$ such that $|A_p^0 - A_p^{j_i}|$ is the i-th largest element in E
 9: **for** i from 1 to n **do**
10:    $S \leftarrow S_0$; $A_p^{\texttt{best}} \leftarrow 0$
11:    **for** $v \in R_{j_i}$ **do**
12:        $S[V_{j_i}] \leftarrow v$; $A_p \leftarrow$ `Evaluate`(S)
13:        **if** $A_p > A_p^{\texttt{best}}$ **then**
14:            $S_0 \leftarrow S$; $A_p^{\texttt{best}} \leftarrow A_p$
15: **return** S_0

16: **Function** `Evaluate`(S):
17:    $\delta \leftarrow$ Create a digital trigger using the laser parameters S
18:    $P_{train} \leftarrow$ Create a poisoned training dataset based on T_{train}
19:        with the digital trigger
20:    $\mathcal{M}' \leftarrow$ Train a backdoored model based on $\mathcal{M}$ using the poisoned
21:        training dataset P_{train}
22:    $A \leftarrow$ Measure attack success rate of $\mathcal{M}'$ on the test dataset P_{test}
23:    **return** A

---

eters remain unchanged. Using those values, another victim model is trained (called perturbed model hereafter), and the impact factor of this laser parameter is defined as the absolute difference of the attack success rate between the perturbed model A_p^i and the baseline one A_p^0. Finally, the optimization order is defined as the descending order of the impact factor, indicating that the laser parameter with a larger impact factor will be optimized first in the next phase.

In the second phase, we iterate the laser parameters in the optimization order obtained in the first phase. The optimized value of each laser parameter is set to the one that is within the valid range of this laser parameter and yields the highest attack success rate. Note that when optimizing one laser parameter, all its previous laser parameters are set to their optimal values.

Algorithm 1 will be utilized to optimize four laser parameters, namely, the scaling ratio, transparency, pasting position, and center brightness (cf. Section 4.2 for details). The adversary uses a local model in Algorithm 1 to optimize laser parameters, which are then used to create and release the poisoned dataset that will be used to train victim models. In experiments, we first optimize laser parameters using the target model, assuming the adversary's knowledge of the

target model (cf. Section 3.1). We then relax this assumption by studying model shift, demonstrating the transferability of optimized parameters from a local model to a different target model.

4   Experimental Settings

Here we present the datasets, trigger settings, models and evaluation metrics.

4.1   Datasets

The datasets used in our experiments are the open-source dataset TT100K [56] and our self-collected dataset LaserMark.

TT100K The TT100K dataset [56] is used to generate the clean training dataset T_{train}, the clean test dataset T_{test}, and the poisoned training dataset P_{train}. The TT100K dataset consists of street view images taken in China, each of which contains one or more road traffic signs and bounding-boxes to locate the traffic signs. Leveraging the bounding box information and excluding the traffic sign categories with less than 16 training images, we extracted 16,130 and 7,969 clean training traffic sign images and test traffic sign images, respectively, each of which belongs to one of 66 categories. We then randomly select 5% (i.e., 806 out of 16,130) images (T_{select}) from the clean training dataset T_{train}, paste a digital trigger to each of the selected images in T_{select}, and modify their labels to the target traffic sign label. The 5% ratio is lower than or equal to that of previous works [9, 17, 38, 47]. Using a larger ratio will make the attack more powerful [17, 46, 47]. Finally, the poisoned images and the clean training images from T_{train} are merged to form the poisoned training dataset P_{train}.

LaserMark Motivation. Our attack features physical backdoor attacks, so traffic sign images with physical laser-based triggers are required to evaluate its effectiveness. However, to the best of our knowledge, no such dataset is available. To fill this gap, we collect and release LaserMark, the *first* dataset containing traffic sign images with physical laser spots as backdoor triggers, hoping that it will foster further research on physical attacks against autonomous driving. Below, we present the collection setup and the details of LaserMark.

Hardware setup. To emit laser spots, we used laser pointers, one kind of civil portable laser transmitters, since they are easy to obtain from markets at a low price and easy to carry and switch, thus enabling convenient and low-cost attack deployment. Specifically, we adopt three laser pointers that differ in the color and shape of their emitted laser spots, i.e., red, green, and blue colors, and circle, and rectangle shapes, respectively, whose laser spots are shown in Fig. 2. The size of their laser spots on the illuminated objects can be adjusted via configured buttons. We use iPhone 12 mini as the photographing device to capture the traffic signs, simulating the shooting functionality of vehicle cameras.
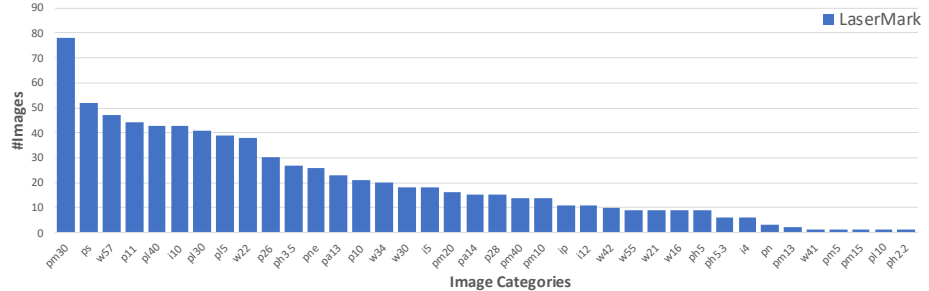
Fig. 3: The number of images contained in each category of LaserMark. Image categories refer to `https://cg.cs.tsinghua.edu.cn/traffic-sign`.

Environment setup. Two operators collaboratively collected the images in China's urban streets. The laser pointer is equipped with a button to adjust the focus of the laser spot. The size of the spot projected onto traffic signs depends on both the focus setting and the pointer's (adversary's) distance from the signs. In practice, the adversary can adjust the focus based on their distance to achieve a laser spot size resulting in a clear projection on the traffic signs, called reasonable size. Therefore, one operator holds the laser pointer more than 30 meters away from the traffic sign and adjusts the laser spot to a reasonable size. The other operator photographs the traffic signs with the photographing device from 5 to 30 meters in front of the traffic sign and 1.5 meters off the ground. To collect more diverse images, we adjusted the angle and distance between the laser pointer and the photographing device and collect 2–5 images per setting. During the collection, we avoided projecting the lasers to those areas of traffic signs that will impact their visibility, e.g., areas with black-color text.

Open-source LaserMark. After collection, we appropriately cropped each image so that the traffic sign is complete, centered, and occupy most of the pixel space. Finally, we have 676 road traffic sign images with physical laser-based triggers, among which 235, 224, and 217 images have red, green, and blue laser points, respectively. These traffic sign images constitute the poisoned test dataset P_{test}, which will be used to evaluate the attack success rate in our experiments.

In addition to the poisoned physical images P_{test} with physical triggers, we also collect 158 clean physical images without physical triggers and add them into the clean test dataset T_{test}. In total, we have 834 images, covering 32 different traffic sign categories, where the number of images contained in each category of LaserMark is shown in Fig. 3 and some examples contained in LaserMark are shown in Fig. 4. They are published as an open-source dataset.

4.2   Trigger Settings

As mentioned in Section 3.2, we propose an effective approach to optimize the parameters of the digital triggers toward a more powerful physical backdoor attack. The laser pointer typically includes a focus adjustment button, which

Fig. 4: Examples of images included in LaserMark.

affects the size and center brightness of the laser spot. Adversaries can freely project the laser spot onto any position of a traffic sign, and stronger natural light makes the spot appear more transparent. These factors motivate us to optimize the four parameters associated with the size, transparency, location, and center brightness of laser spots.

Scale parameter K, defined as $K = \frac{max\{W,H\}}{S}$, represents the size of the laser spot relative to the size of the traffic sign image, where $W \times H$ is the size of the bounding box of the traffic sign, and S is the length of radius and semi-major axis for circular and rectangular laser spot, respectively. We range K from 2 to 14 with the step of 1. We do not define K as the ratio of areas between the bounding box and laser spot since when the length and width of the bounding box are uneven, the laser spot will be too small even when K is set to 1.

Opacity parameter W controls the opacity of the laser spot, where the smaller the opacity parameter W is, the more transparent the laser spot is. We range W from 15 to 255 with the step of 15, where $W = 255$ represents the original trigger. A trigger with the opacity parameter W is achieved by multiplying each pixel of the original trigger by $\frac{W}{255}$.

Location parameter L controls the location of the laser spot with respect to the traffic sign. We consider two types of location, namely, *Center* and *Random*, i.e., the trigger is placed at the geometric center and a random location of the traffic sign, respectively.

Highlight parameter H is a binary parameter, where the center of the trigger is highlighted when $H = 1$, and it is not highlighted when $H = 0$. We highlight the center by increasing the pixel value of the central area.

All these parameters of digital laser-based triggers can be controlled by simple geometric drawing operations, i.e., scaling, pixel value alteration, and shift.

4.3   Models

In this work, we demonstrate the effectiveness of our laser-based physical attack on the traffic sign recognition task. We adopt the ResNet-34 model [18] as the victim model, and train the model for 200 epochs using the SGD optimizer with the momentum of 0.9, weight decay of 5×10^{-4}, batch size of 32, and learning rate of 0.01. To overcome the randomness, we will evaluate our attack on the models obtained at the training epochs 100, 120, 160, 180, and 200, and report

the average results. In the ablation study, we also evaluate the effectiveness of our attack on the ViT [13], GoogLeNet [41], and Yolo-V8 [1] models.

4.4   Evaluation Metrics

We evaluate the performance of our attack using two standard metrics: (1) **Clean accuracy** A_c: the accuracy of the victim model on the clean test dataset T_{test}. It quantifies the effect of our attack on normal traffic sign images and the stealthiness of our attack. (2) **Attack success rate** A_p: the portion of traffic sign images with physical triggers in the poisoned test dataset P_{test} that can be classified as the specified target label. We select the "stop and yield" sign as the target label and remove all the genuine "stop and yield" images from the dataset P_{test} when computing A_p to avoid bias. For comparison, we also denote A_{cn} and $A_{pn}$the accuracy and attack success rate on the normal model trained with the clean training dataset.

Table 2: Values of each laser parameter for the baseline model, perturbed models, and optimized models. C and R are short for *Center* and *Random*, respectively.

	Baseline				Perturbed				Optimize L				Optimize K				Optimize W				Optimize H			
	L	K	W	H	L	K	W	H	L	K	W	H	L	K	W	H	L	K	W	H	L	K	W	H
Red	C	6	90	0	R	8	120	1	R	6	90	0	R	6	90	0	R	6	90	0	R	6	90	1
Green	C	6	90	0	R	8	120	1	R	6	90	0	R	6	90	0	R	6	60	0	R	6	60	1
Blue	C	6	90	0	R	8	120	1	R	6	90	0	R	4	90	0	R	4	150	0	R	4	150	0

5   Experimental Results

In this section, we first evaluate a baseline attack and the optimized attack with the laser parameter optimization approach, then the many-to-one and many-to-many variants of LASERGUIDER, and finally perform ablation studies to confirm the significance of the order of optimizing laser parameters, the model transferability of optimized laser parameters, and the effectiveness of using digital triggers to simulate physical triggers when constructing a poisoned training dataset.

5.1   Baseline Attack

Settings. Regarding the values of the four laser parameters, we set $K = 6$, $W = 90$, $L = Center$, and $H = 0$ as a baseline attack (cf. Table 2). The digital backdoor triggers are created using these values which in turn are used to generate the poisoned training dataset P_{train}. We then train the victim model using the poisoned training dataset P_{train} and finally calculate the clean accuracy A_c on the clean test dataset T_{test} and the attack success rate A_p on the poisoned
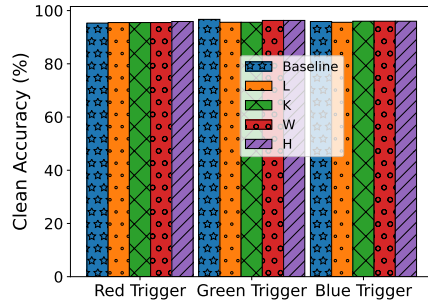
Fig. 5: The clean accuracy A_c of the baseline attack and the attack with each optimized laser parameter.
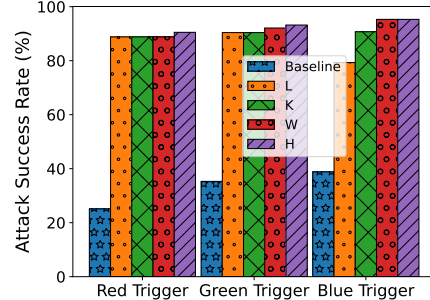
Fig. 6: The attack success rate A_p of the baseline attack and the attack with each optimized laser parameter.

test dataset P_{test}. The baseline attack is conducted independently for each of three types of triggers and the physical trigger used in the poisoned test dataset P_{test} has the same shape and color as the digital backdoor trigger used in the poisoned training dataset P_{train}. For comparison, we also train a normal model using the clean training dataset T_{train}, which yields 96.8% clean accuracy A_{cn} and 0% attack success rate A_{pn}.

Results. The clean accuracy A_c and the attack success rate A_p of the victim models with different types of triggers are shown in Fig. 5 and Fig. 6, respectively. These models achieve more than 95% clean accuracy A_c, very close to the clean accuracy A_c of the normal model (i.e., 96.8%), regardless of the type of triggers, indicating our attack has negligible effects on the normal input images. While our baseline attack is effective, the attack success rate of our baseline attack is lower than 40%. Below, we will show that our laser parameter optimization approach can significantly improve the attack success rate by a large margin.

5.2   Optimized Attack

Optimization order. The first phase of our approach is to determine the optimization order of the four laser parameters based on the difference of the attack success rate between the baseline and perturbed models. We set $K = 8$, $W = 120$, $L = Random$, and $H = 1$ for the perturbed models (cf. Table 2). The comparison of the attack success rate between the baseline and each perturbed model is shown in Fig. 7. We can observe that the attack success rate A_p of each perturbed model either increases or decreases compared to the baseline model, although the degree of change (i.e., impact factor) varies. We find that the order of the impact factor remains consistent across different types of triggers, i.e., L has the largest impact factor, followed by K, W, and H. This confirms our previous hypothesis that the degree of impacts on the attack success rate varies with parameters.

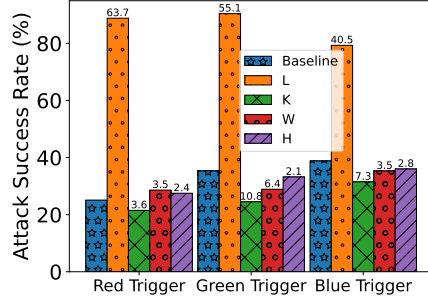Below, we optimize the parameters one by one in the order L, K, W, and H.

Fig. 7: Attack success rate A_p of baseline and perturbed models, where the above-bar digit denotes the absolute difference of A_p between the baseline and each perturbed model.
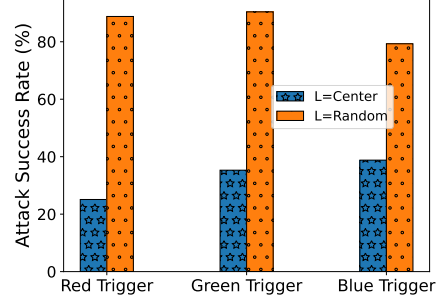
Fig. 8: The attack success rate A_p with respect to the value of the location parameter L.

Optimizing the location parameter L. We traverse the value range of the location parameter L (i.e. $\{Center, Random\}$). The attack success rate with respect to the value of L is shown in Fig. 8. We can observe that a random position is more effective than a center position, regardless of the type of triggers. This is because random digital trigger position enables the backdoored model to learn a mapping from the trigger to the target label independent on the trigger position. This benefits physical attacks where the position of physical triggers is flexible. Therefore, we set $L = Random$ for all the three types of triggers.

Optimizing the scale parameter K. We traverse the value range of the scale parameter K, from 2 to 14 with the step of 1. Fig. 9 depicts the clean accuracy A_c and attack success rate A_p varying in the scale parameter K. In general, the attack success rate A_p first increases and then decreases with respect to the scale parameter K, indicating that both too small and too large digital triggers have negative impact on the attack success rate. This is because a trigger of small size may be overlooked by the model and a trigger of large size may cover some critical image areas and influence the semantics of images (cf. Section 6.1), causing the victim model to recognize them as other labels rather than the target label. The optimal values of the scale parameter K are set as 4, 6, and 6 for the blue, green, and red triggers, respectively, where they achieve the highest attack success rate A_p.

Optimizing the opacity parameter W. We traverse the value range of the opacity parameter W, from 15 to 255 with the step of 15. Fig. 10 demonstrates how accuracy changes with respect to the opacity parameter W. We find that the attack success rate A_p of the red and green triggers does not monotonically change with respect to the opacity parameter W. We conjecture that this is because a transparent trigger (small W) is more likely to be overlooked by the model, while a trigger with high opacity (large W) may influence the image semantics. Specifically, the red, green, and blue triggers achieve the highest attack
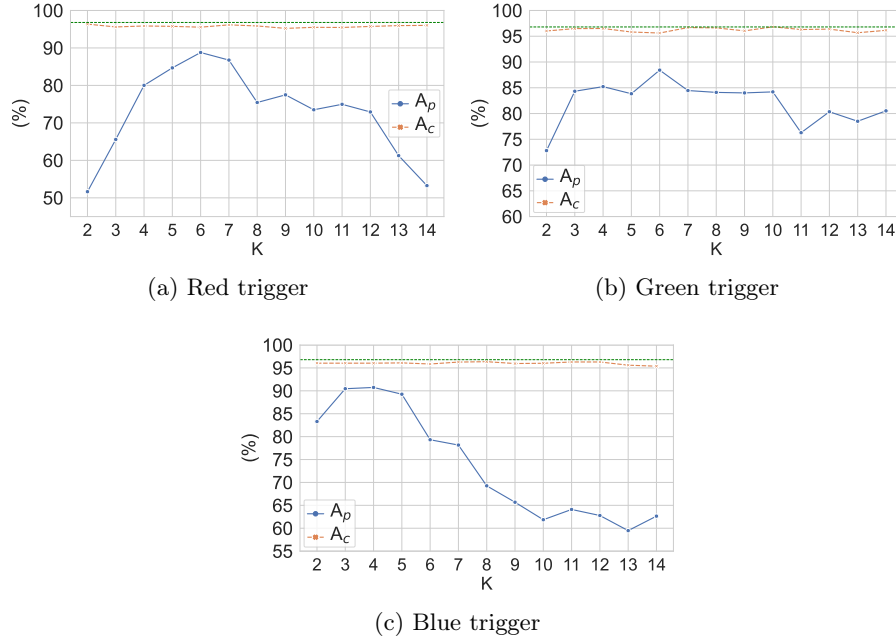
(a) Red trigger

(b) Green trigger

(c) Blue trigger

Fig. 9: The clean accuracy A_c and attack success rate A_p with respect to the value of the scale parameter K.

success rate A_p when $W = 90$, $W = 60$, and $W = 150$, respectively, which are set as the optimal values of the opacity parameter W.

Optimizing the highlighting parameter H. Similarly, we traverse the value range of the highlighting parameter H, i.e., $\{0, 1\}$. Fig. 11 compares the attack success rate A_p between when $H = 0$ (trigger center not highlighted) and $H = 1$ (trigger center highlighted). We find that the red and green triggers achieve a higher attack success rate A_p when $H = 1$, while the blue trigger achieves a higher attack success rate A_p when $H = 0$. The difference is probably due to their different shapes. Accordingly, we set $H = 0$ for the blue trigger and $H = 1$ for the other two types of triggers.

Final Attack. Table 2 shows the final optimized value of each parameter. Fig. 5 and Fig. 6 show the clean accuracy and the attack success rate of the baseline attack and the attack with iteratively optimized parameter in the order L, K, W, and H, respectively. We can observe that during the step-by-step optimization in the order L, K, W, and H, the attack success rate A_p generally keeps increasing, while the clean accuracy A_c remains stable and decreases no more than 0.4% throughout the optimization process. Our final optimized attack achieves the attack success rate of 90.5%, 93.2%, and 95.3% on the red, green, and blue triggers,
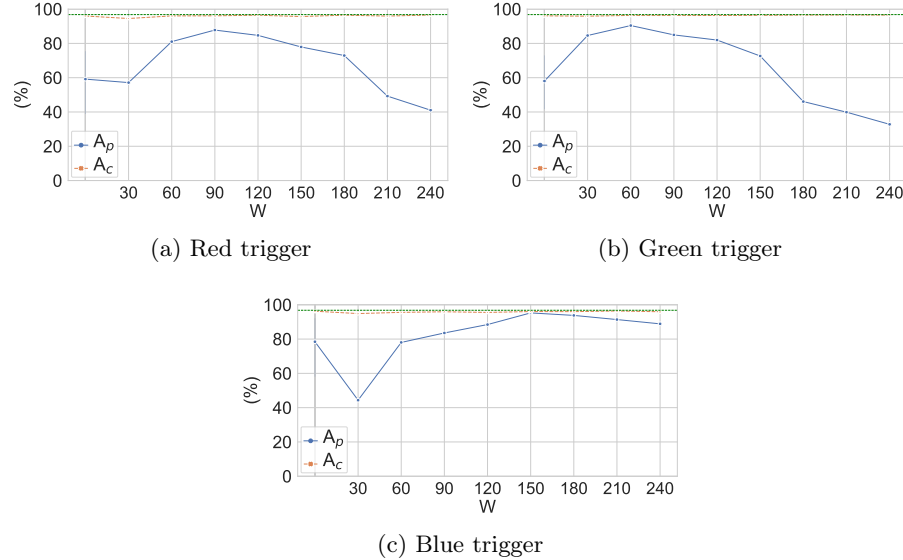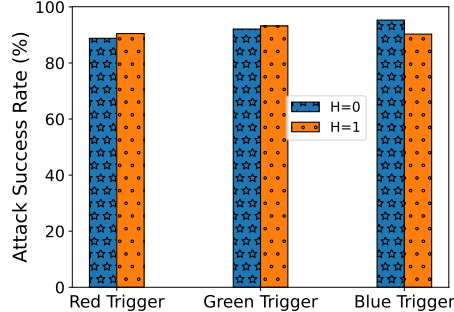
(a) Red trigger

(b) Green trigger

(c) Blue trigger

Fig. 10: The clean accuracy A_c and attack success rate A_p with respect to the value of the opacity parameter W.

respectively, significantly higher than the baseline attack. These demonstrate the effectiveness of the optimization approach and our attack LASERGUIDER.

5.3 Many-to-One Attack

Previous experiments confirmed the effectiveness of LASERGUIDER when there is one designated trigger and one corresponding target label (i.e., one-to-one attack). Here, we demonstrate the capability of LASERGUIDER for many-to-one attack where the adversary specifies k different triggers while associates them with the same target label. Without loss of generalizability, we set $k = 2$. To train the backdoored model, we first randomly partition the set of randomly selected clean images T_{select} (5% of the clean training dataset T_{train}) into two parts containing nearly identical number of samples, then add red trigger and green trigger to the two parts, respectively, and finally modify the labels of all poisoned images to "stop and yield". The trigger parameters are set as the optimal values found in Section 5.2. The results are shown in Table 3. Although the red and green triggers have the same shape, the one-to-one attack has no more than 5% attack success rate on the images with different trigger and target label from that involved in training. In contrast, although the poisoning rate is reduced from 5% to 2.5% for each physical trigger, the many-to-one attack is able to achieve 85.6% and 89.2% attack success rate on the red and green physical triggers, respectively. Also, compared to the one-to-one attack, the clean accu-

Fig. 11: Attack success rate A_p w.r.t. the value of the highlighting parameter H.

Table 3: Results of many-to-one and many-to-many attacks, where ps and $il100$ are short for "stop and yield" and "speed limi" signs, respectively.

Test ⟍ Train	A_c	red $\to ps$	green $\to ps$	green $\to il100$
One-to-one (red $\to ps$)	96.8%	90.5%	5%	2.5%
One-to-one (green $\to ps$)	96.4%	2%	93.2%	1.0%
Many-to-one (red $\to ps$) & (green $\to ps$)	96.0%	85.6%	89.2%	N/A
Many-to-many (red $\to ps$) & (green $\to il100$)	95.0%	80.3%	N/A	84.9%

racy A_c of the many-to-one attack only decreases by 0.8%. These demonstrates the capability of LASERGUIDER in achieving many-to-one backdoor attacks.

5.4   Many-to-Many Attack

We also demonstrate the capability of LASERGUIDER in launching the many-to-many backdoor attack where the adversary specifies k different triggers each of which is associated with a distinct target label. We also set $k = 2$, and the process of model training is the same as in Section 5.3 except that we set the "stop and yield" label and "speed limit" label for the red and green triggers, respectively. The results are shown in Table 3. The many-to-many attack achieves 84.9% attack success rate on the green physical trigger, much higher than that of the one-to-one attack on "green $\to il100$". Also, the clean accuracy A_c of the many-to-many attack decreases only by 1.8%, compared to the one-to-one attack. These demonstrate the capability of LASERGUIDER in achieving many-to-many backdoor attacks. However, the attack success rate of the many-to-many attack on the red trigger is slightly lower than that of the one-to-one attack on "red $\to ps$", because the poisoning rate is reduced from 5% to 2.5%.

Table 4: The attack success rate A_p and clean accuracy A_c with the swapped optimization order.

	Red	Green	Blue
A_p (original)	90.5%	93.2%	95.3%
A_p (swapped)	87.1%↓	90.1%↓	95.3%−
A_c (original)	95.9%	96.3%	96.0%
A_c (swapped)	95.8%↓	96.3%−	96.0%−

Table 5: Final optimized laser parameter with swapped optimization order. Text in red highlights change compared to original order.

	L	K	W	H
Red (original)	Random	6	90	1
Red (swapped)	Random	5	90	0
Green (original)	Random	6	60	1
Green (swapped)	Random	7	75	0
Blue (original)	Random	4	150	0
Blue (swapped)	Random	4	150	0

5.5   Ablation Study

In this subsection, we perform ablation experiments to further evaluate the effectiveness of the proposed optimization method and the poisoned training dataset construction method by utilizing digital triggers to simulate the physical triggers.

Swapping optimization order. To validate the necessity of determining the laser parameter optimization order, we run the attack with an intentionally swapped optimization order. Specifically, we randomly swapped the optimization order of the location parameter L and the scale parameter K, i.e. optimizing the attack with the order K, L, W, and H, instead of the order L, K, W, and H. As shown in Table 4, the attack success rate A_p decreases on the red and green triggers, and the clean accuracy A_c decreases on the red trigger. These demonstrate the significance of using appropriate optimization order and the effectiveness of the optimization order determining method used in our optimization approach. We notice that A_p and A_c remain unchanged for the blue backdoor because the optimized values of all parameters for this trigger do not change (cf. Table 5).

Model transferability. Previously, we assumed that the attacker can optimize the laser parameters on the target DNN model. To relax this assumption, we investigate the transferability of our approach by (1) applying the laser parameter values *in each step* during the optimization process obtained on the ResNet model to ViT [13] and GoogLeNet [41] models. The results are reported in Table 6 and Table 7. Similar to the ResNet model, the attack success rate A_p keeps increasing on at least one trigger, and finally, the optimized attack achieves a much higher attack success rate A_p than the baseline attack; (2) applying the *final* optimized laser parameters obtained on ResNet to Yolo-V8 [1], achieving the attack success rate of 83.2%, 88.2%, and 96.54% with the red, green, and blue

Table 6: Attack success rate A_p of the victim model ViT at each step during the optimization process.

	Red	Green	Blue
Baseline	31.3%	52.3%	58.1%
L	62.4%↑	87.6%↑	63.2%↑
K	62.4%−	87.6%−	98.1%↑
W	62.4%−	88.1%↑	99.5%↑
H	70.7%↑	90.3%↑	99.5%−

Table 7: Attack success rate A_p of GoogLeNet at each step during laser parameters optimization.

	Red	Green	Blue
Baseline	40.7%	48.1%	57.2%
L	81.5%↑	83.8%↑	70.9%↑
K	81.5%−	83.8%−	76.4%↑
W	81.5%−	85.3%↑	89.8%↑
H	85.3%↑	88.8%↑	89.8%−

triggers, respectively. These results confirm the generability of the optimized laser parameter, the model transferability of our laser parameters optimization approach, and our attack's effectiveness across different models.

Replacing digital triggers with physical ones. To reduce attack overhead, we simulate physical triggers with digital ones for constructing poisoned training datasets. Here we compare the attack effectiveness between using digital triggers alone and including physical triggers. For each trigger, we replace the digital trigger with its physical counterpart in M randomly selected images from P_{train}, with M ranging from 10 to 50. As shown in Fig. 12, attacks using physical triggers in the training dataset consistently achieve lower success rates than those using only digital triggers, likely because digital triggers can simulate a broader range of physical triggers due to easier parameter control. This demonstrates the effectiveness of utilizing digital triggers to simulate the physical triggers when constructing the poisoned training dataset.

6   Discussion

6.1   Failure Analysis

While our attack can achieve high success rate, there are still few cases on which LASERGUIDER fails. After analyzing the failed cases, we find that the failures are mainly due to the following two reasons: (1) **Triggers changing semantics.** We notice that sometimes an embedded trigger can change the image semantics from the original traffic sign to another traffic sign. For instance, an overexposed blue trigger, e.g., Fig. 13 (left), looks like a slanted arrow in the "Motor vehicle lane" sign as shown in Fig. 13 (right). As a result, the victim model will classify
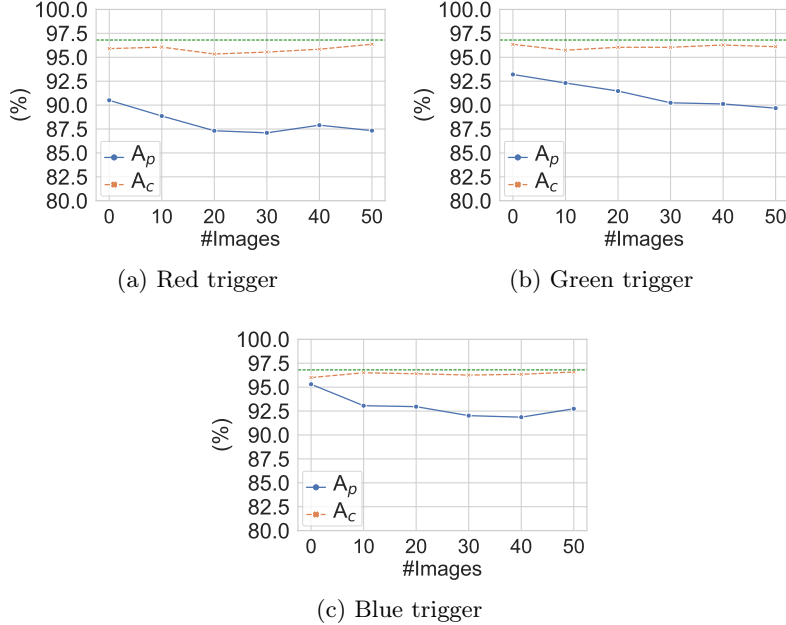
(a) Red trigger

(b) Green trigger

(c) Blue trigger

Fig. 12: The clean accuracy A_c and attack success rate A_p with respect to the number of poisoned training images with the physical triggers. #Images=0 denotes only using digital triggers when constructing the poisoned training dataset.

it to the "Motor vehicle lane" sign rather than our target label. (2) **Bad trigger quality.** When a trigger is too bright or too dim, e.g., as demonstrated in Fig. 14, they got unnoticed by the victim model, leading to a failed attack.

Fig. 13: Trigger changing semantics

Fig. 14: Bad trigger quality

6.2   Countermeasure

We consider five defenses. The former four from prior works were shown promising and the last one is our designed adaptive defense. While they vary from

backdoor detection [45] to poison data detection [6, 43], run-time trigger detection [15] and removal, LASERGUIDER shows robustness against all of them, urging for more effective defenses to mitigate laser physical backdoor attacks.

Neural Cleanse (NC) [45] deems a model backdoored if a label requires much smaller norm of modifications to classify all examples into it. Applied to our attack, 95% of unaffected labels have smaller norms than the target label, indicating NC's unreliability. This is due to the larger laser spot size compared to sticker-based triggers [16], resulting in a higher norm for the target label.

Activation Clustering (AC) [6] assumes that inputs with triggers activate distinct neurons from clean inputs, detecting poisoned training data by comparing activation patterns. Applied to LASERGUIDER, AC yields a 90% false negative rate and 29% false positive rate, likely due to significant overlap in neuron activation between inputs with laser-based triggers and clean inputs.

Spectral Signatures (SS) [43] observes that inputs with triggers exhibit differences in the covariance spectrum of neural network feature representations compared to clean inputs, using statistical methods like SVD to detect outliers (poisoned data). However, it identifies only 8% of poisoned samples for LASER-GUIDER, indicating that our attack remains a potent real-world threat.

STRIP [15] blends an inference input with random clean inputs and flags it as containing triggers if its output randomness (entropy) is below a threshold (set for a 5% false positive rate per [47]). Applied to LASERGUIDER, STRIP fails to detect 63% of triggered inputs, likely due to the diversity of physical laser-based triggers, which maintain high output randomness even after blending.

Laser Removal (LR) uses prior knowledge of the laser spot's color and shape to mask matching regions and replace them with pixel interpolation. The attack success rate is reduced but still relatively high (over 48%), since inconsistencies in shape and color caused by extreme projection angles and lighting distortions leave many spots undetected. Additionally, misidentifying traffic sign areas as spots reduces normal accuracy by 14%. These indicate that it is challenging to mitigate physical triggers without affecting normal accuracy [23].

7   Conclusion

In this work, we designed laser-based physical triggers and proposed LASER-GUIDER, a novel laser-driven backdoor attack targeting deep neural networks. Leveraging lasers' long-distance transmission and instant imaging capabilities, LASERGUIDER achieves remote control, high temporal stealthiness, and superior flexibility and mobility, addressing the limitations of existing backdoor methods. To enhance attack performance, we introduced an effective parameter selection method for laser-based triggers. Experiments on traffic sign recognition models, using both open-source and our collected real-world datasets, demonstrate the high effectiveness of LASERGUIDER, negligible impact on normal inputs, and the effectiveness of the optimization approach. Our work sheds light on more practical and feasible physical backdoor attacks and contributes the first traffic sign dataset featuring physical laser triggers to advance research in this domain.

Disclosure of Interests. The authors have no competing interests to declare that are relevant to the content of this article.

References

1. Explore Ultralytics YOLOv8: A new state-of-the-art in computer vision, supporting object detection, classification, and segmentation tasks. (2019)
2. Bakator, M., Radosav, D.: Deep learning and medical diagnosis: A review of literature. Multimodal Technol. Interact. **2**(3), 47 (2018)
3. Balasubramaniam, S., Joe, C.V., Sivakumar, T.A., Prasanth, A., Kumar, K.S., Kavitha, V., Dhanaraj, R.K.: Optimization enabled deep learning-based ddos attack detection in cloud computing. Int. J. Intell. Syst. **2023**, 1–16 (2023)
4. Barni, M., Kallas, K., Tondi, B.: A new backdoor attack in CNNS by training set corruption without label poisoning. In: ICIP (2019)
5. Carlini, N., Athalye, A., Papernot, N., Brendel, W., Rauber, J., Tsipras, D., Goodfellow, I.J., Madry, A., Kurakin, A.: On evaluating adversarial robustness. CoRR **abs/1902.06705** (2019)
6. Chen, B., Carvalho, W., Baracaldo, N., Ludwig, H., Edwards, B., Lee, T., Molloy, I.M., Srivastava, B.: Detecting backdoor attacks on deep neural networks by activation clustering. In: Workshop on Artificial Intelligence Safety. vol. 2301 (2019)
7. Chen, X., Liu, C., Li, B., Lu, K., Song, D.: Targeted backdoor attacks on deep learning systems using data poisoning. CoRR **abs/1712.05526** (2017)
8. Chen, Y., Ye, Z., Zhao, H., Wang, Y.: Feature-based graph backdoor attack in the node classification task. Int. J. Intell. Syst. **2023**, 1–13 (2023)
9. Conti, M., Farronato, N., Koffas, S., Pajola, L., Picek, S.: Invisible threats: Backdoor attack in OCR systems. CoRR **abs/2310.08259** (2023)
10. Doan, K.D., Lao, Y., Zhao, W., Li, P.: LIRA: learnable, imperceptible and robust backdoor attacks. In: Proceedings of the International Conference on Computer Vision. pp. 11946–11956 (2021)
11. Dong, T., Zhang, Z., Qiu, H., Zhang, T., Li, H., Wang, T.: Mind your heart: Stealthy backdoor attack on dynamic deep neural network in edge computing. In: IEEE INFOCOM 2023 - IEEE Conference on Computer Communications, New York City, NY, USA, May 17-20, 2023. pp. 1–10 (2023)
12. Dong, Y., Yang, X., Deng, Z., Pang, T., Xiao, Z., Su, H., Zhu, J.: Black-box detection of backdoor attacks with limited information and data. In: ICCV (2021)
13. Dosovitskiy, A., Beyer, L., Kolesnikov, A., Weissenborn, D., Zhai, X., Unterthiner, T., Dehghani, M., Minderer, M., Heigold, G., Gelly, S., Uszkoreit, J., Houlsby, N.: An image is worth 16x16 words: Transformers for image recognition at scale. In: 9th International Conference on Learning Representations, ICLR (2021)
14. Duan, R., Mao, X., Qin, A.K., Chen, Y., Ye, S., He, Y., Yang, Y.: Adversarial laser beam: Effective physical-world attack to dnns in a blink. In: Proceedings of the IEEE/CVF Conference on Computer Vision and Pattern Recognition. pp. 16062–16071 (2021)

15. Gao, Y., Xu, C., Wang, D., Chen, S., Ranasinghe, D.C., Nepal, S.: STRIP: a defence against trojan attacks on deep neural networks. In: Proceedings of the 35th Annual Computer Security Applications Conference, ACSAC 2019, San Juan, PR, USA, December 09-13, 2019. pp. 113–125 (2019)
16. Gu, T., Dolan-Gavitt, B., Garg, S.: Badnets: Identifying vulnerabilities in the machine learning model supply chain. CoRR **abs/1708.06733** (2017)
17. Han, X., Xu, G., Zhou, Y., Yang, X., Li, J., Zhang, T.: Physical backdoor attacks to lane detection systems in autonomous driving. In: The 30th ACM International Conference on Multimedia (2022)
18. He, K., Zhang, X., Ren, S., Sun, J.: Deep residual learning for image recognition. In: IEEE Conference on Computer Vision and Pattern Recognition, CVPR. pp. 770–778 (2016)
19. He, Y., Shen, Z., Xia, C., Hua, J., Tong, W., Zhong, S.: SGBA: A stealthy scapegoat backdoor attack against deep neural networks. Comput. Secur. **136**, 103523 (2024)
20. Huang, Y., Shih, L., Tsai, C., Shen, G.: Describing video scenarios using deep learning techniques. Int. J. Intell. Syst. **36**(6), 2465–2490 (2021)
21. Huang, Y., Chen, Y.: Autonomous driving with deep learning: A survey of state-of-art technologies. CoRR **abs/2006.06091** (2020)
22. Kingma, D.P., Ba, J.: Adam: A method for stochastic optimization. In: ICLR (2015)
23. Li, H., Wang, Y., Xie, X., Liu, Y., Wang, S., Wan, R., Chau, L., Kot, A.C.: Light can hack your face! black-box backdoor attack on face recognition systems. CoRR **abs/2009.06996** (2020)
24. Li, Q., Chen, W., Xu, X., Zhang, Y., Wu, L.: Precision strike: Precise backdoor attack with dynamic trigger. Comput. Secur. **148**, 104101 (2025)
25. Li, Y., Jiang, Y., Li, Z., Xia, S.T.: Backdoor learning: A survey. IEEE Transactions on Neural Networks and Learning Systems (2022)
26. Li, Y., Zhai, T., Jiang, Y., Li, Z., Xia, S.: Backdoor attack in the physical world. CoRR **abs/2104.02361** (2021)
27. Lian, W., Zhang, Y., Chen, X., Jia, B., Zhang, X.: Ipcadp-equalizer: An improved multibalance privacy preservation scheme against backdoor attacks in federated learning. Int. J. Intell. Syst. **2023**, 1–20 (2023)
28. Lin, J., Xu, L., Liu, Y., Zhang, X.: Composite backdoor attack for deep neural network by mixing existing benign features. In: ACM SIGSAC Conference on Computer and Communications Security. pp. 113–131 (2020)
29. Liu, Y., Ma, S., Aafer, Y., Lee, W., Zhai, J., Wang, W., Zhang, X.: Trojaning attack on neural networks. In: 25th Annual Network and Distributed System Security Symposium, NDSS (2018)
30. Liu, Y., Ma, X., Bailey, J., Lu, F.: Reflection backdoor: A natural backdoor attack on deep neural networks. In: European Conference on Computer Vision. vol. 12355, pp. 182–199 (2020)
31. Liu, Y., Xie, Y., Srivastava, A.: Neural trojans. In: 2017 IEEE International Conference on Computer Design. pp. 45–48. IEEE (2017)
32. Mehrish, A., Majumder, N., Bharadwaj, R., Mihalcea, R., Poria, S.: A review of deep learning techniques for speech processing. Information Fusion **99**, 101869 (2023)
33. Nguyen, T.A., Tran, A.T.: Input-aware dynamic backdoor attack. In: Annual Conference on Neural Information Processing Systems (2020)
34. Oyama, T., Okura, S., Yoshida, K., Fujino, T.: Backdoor attack on deep neural networks triggered by fault injection attack on image sensor interface. Sensors **23**(10), 4742 (2023)

35. Pan, X., Zhang, M., Sheng, B., Zhu, J., Yang, M.: Hidden trigger backdoor attack on NLP models via linguistic style manipulation. In: 31st USENIX Security Symposium. pp. 3611–3628 (2022)
36. Rakin, A.S., He, Z., Fan, D.: Tbt: Targeted neural network attack with bit trojan. In: Proceedings of the IEEE/CVF Conference on Computer Vision and Pattern Recognition. pp. 13198–13207 (2020)
37. Rehman, H., Ekelhart, A., Mayer, R.: Backdoor attacks in neural networks - A systematic evaluation on multiple traffic sign datasets. In: CD-MAKE. Lecture Notes in Computer Science (2019)
38. Sun, W., Jiang, X., Li, D., Zhao, C.: Diffphysba: Diffusion-based physical backdoor attack against person re-identification in real-world. arXiv preprint arXiv:2405.19990 (2024)
39. Sun, Z., Du, X., Song, F., Li, L.: Codemark: Imperceptible watermarking for code datasets against neural code completion models. In: Chandra, S., Blincoe, K., Tonella, P. (eds.) Proceedings of the 31st ACM Joint European Software Engineering Conference and Symposium on the Foundations of Software Engineering (ESEC/FSE). pp. 1561–1572 (2023)
40. Sun, Z., Du, X., Song, F., Ni, M., Li, L.: Coprotector: Protect open-source code against unauthorized training usage with data poisoning. In: The ACM Web Conference. pp. 652–660 (2022)
41. Szegedy, C., Liu, W., Jia, Y., Sermanet, P., Reed, S.E., Anguelov, D., Erhan, D., Vanhoucke, V., Rabinovich, A.: Going deeper with convolutions. In: IEEE Conference on Computer Vision and Pattern Recognition, CVPR. pp. 1–9 (2015)
42. Tang, R., Du, M., Liu, N., Yang, F., Hu, X.: An embarrassingly simple approach for trojan attack in deep neural networks. In: Proceedings of the 26th ACM SIGKDD International Conference on Knowledge Discovery & Data Mining. pp. 218–228 (2020)
43. Tran, B., Li, J., Madry, A.: Spectral signatures in backdoor attacks. In: Advances in Neural Information Processing Systems 31: Annual Conference on Neural Information Processing Systems 2018, NeurIPS 2018, December 3-8, 2018, Montréal, Canada. pp. 8011–8021 (2018)
44. Turner, A., Tsipras, D., Madry, A.: Label-consistent backdoor attacks. CoRR **abs/1912.02771** (2019)
45. Wang, B., Yao, Y., Shan, S., Li, H., Viswanath, B., Zheng, H., Zhao, B.Y.: Neural cleanse: Identifying and mitigating backdoor attacks in neural networks. In: IEEE Symposium on Security and Privacy. pp. 707–723. IEEE (2019)
46. Wei, H., Yu, H., Zhang, K., Wang, Z., Zhu, J., Wang, Z.: Moiré backdoor attack (MBA): A novel trigger for pedestrian detectors in the physical world. In: Proceedings of the 31st ACM International Conference on Multimedia (2023)
47. Wenger, E., Passananti, J., Bhagoji, A.N., Yao, Y., Zheng, H., Zhao, B.Y.: Backdoor attacks against deep learning systems in the physical world. In: IEEE Conference on Computer Vision and Pattern Recognition. pp. 6206–6215 (2021)
48. Yao, Y., Li, H., Zheng, H., Zhao, B.Y.: Latent backdoor attacks on deep neural networks. In: CCS. pp. 2041–2055 (2019)
49. Yu, X., Cong, L., Zheng, M., Wang, Y., Liu, X., Shuxiao, S., Yuexuan, M., Jun, Z.: A multitarget backdooring attack on deep neural networks with random location trigger. Int. J. Intell. Syst. **37**(3), 2567–2583 (2022)
50. Zhai, T., Li, Y., Zhang, Z., Wu, B., Jiang, Y., Xia, S.: Backdoor attack against speaker verification. In: IEEE International Conference on Acoustics, Speech and Signal Processing. pp. 2560–2564 (2021)

51. Zhang, X., Liu, A., Zhang, T., Liang, S., Liu, X.: Towards robust physical-world backdoor attacks on lane detection. In: Proceedings of the 32nd ACM International Conference on Multimedia, MM (2024)
52. Zhang, Y., Chen, G., Song, F., Sun, J., Dong, J.S.: Certified quantization strategy synthesis for neural networks. In: 26th International Symposium on Formal Methods. Lecture Notes in Computer Science, vol. 14933, pp. 343–362 (2024)
53. Zhao, Z., Chen, G., Liu, T., Li, T., Song, F., Wang, J., Sun, J.: Attack as detection: Using adversarial attack methods to detect abnormal examples. ACM Trans. Softw. Eng. Methodol. **33**(3), 68:1–68:45 (2024)
54. Zhao, Z., Chen, G., Wang, J., Yang, Y., Song, F., Sun, J.: Attack as defense: characterizing adversarial examples using robustness. In: Cadar, C., Zhang, X. (eds.) Proceedings of the 30th ACM SIGSOFT International Symposium on Software Testing and Analysis (ISSTA). pp. 42–55. ACM (2021)
55. Zhong, H., Liao, C., Squicciarini, A.C., Zhu, S., Miller, D.: Backdoor embedding in convolutional neural network models via invisible perturbation. In: Proceedings of the Tenth ACM Conference on Data and Application Security and Privacy. pp. 97–108 (2020)
56. Zhu, Z., Liang, D., Zhang, S., Huang, X., Li, B., Hu, S.: Traffic-sign detection and classification in the wild. In: Proceedings of the IEEE Conference on Computer Vision and Pattern Recognition. pp. 2110–2118 (2016)